ROM SAF Report 24
Ref: SAF/ROM/METO/REP/RSR/024
Web: www.romsaf.org
Date: 20 June 2016

The EUMETSAT Network of Satellite Application Facilities

ROM SAF
Radio Occultation Meteorology

ROM SAF Report 24

The calculation of planetary boundary layer heights in ROPP

Ian Culverwell

Met Office, Exeter, UK

Document Author Table

	Name	Function	Date	Comments
Prepared by:	I D Culverwell	ROM SAF Project Team	20 June 2016	
Reviewed by:	M Forsythe	Met Office	23 Mar 2016	
Reviewed by:	R Saunders	Met Office	28 Apr 2016	
Approved by:	K B Lauritsen	ROM SAF Project Manager	10 Jun 2016	

Document Change Record

Issue/Revision	Date	By	Description
0.1	8 Feb 2016	IDC	1st draft
0.2	29 Feb 2016	IDC	2nd draft, including some forward modelled results
0.3	10 Mar 2016	IDC	3rd draft, with typos fixed plus a few more details
0.4	11 May 2016	IDC	4th draft, with responses to referees' comments
1.0	20 Jun 2016	IDC	Final version, following review by ROM SAF PM

ROM SAF

The Radio Occultation Meteorology Satellite Application Facility (ROM SAF) is a decentralised processing centre under EUMETSAT which is responsible for operational processing of GRAS radio occultation data from the Metop satellites and RO data from other missions. The ROM SAF delivers bending angle, refractivity, temperature, pressure, and humidity profiles in near-real time and offline for NWP and climate users. The offline profiles are further processed into climate products consisting of gridded monthly zonal means of bending angle, refractivity, temperature, humidity, and geopotential heights together with error descriptions.

The ROM SAF also maintains the Radio Occultation Processing Package (ROPP) which contains software modules that will aid users wishing to process, quality-control and assimilate radio occultation data from any radio occultation mission into NWP and other models.

The ROM SAF Leading Entity is the Danish Meteorological Institute (DMI), with Cooperating Entities: i) European Centre for Medium-Range Weather Forecasts (ECMWF) in Reading, United Kingdom, ii) Institut D'Estudis Espacials de Catalunya (IEEC) in Barcelona, Spain, and iii) Met Office in Exeter, United Kingdom. To get access to our products or to read more about the project please go to: http://www.romsaf.org

Intellectual Property Rights

Abstract

This report concerns the Planetary Boundary Layer Height (PBLH) diagnostics that have been implemented in the ROM SAF's Radio Occultation Processing Package, ROPP. Algorithms for calculating the PBLH are briefly described. PBLHs calculated from six different profile variables — three 'observation fields' and three 'model fields' — are compared and contrasted, both by profile-by-profile scrutiny of selected examples, and by inspection of the average of a month of occultations. PBLHs derived from forward modelled background fields are also briefly considered. Tentative conclusions are drawn before possible future work is considered.

Contents

1 Introduction

The atmospheric boundary layer bridges the gap between the Earth's surface and the free troposphere, and therefore plays a key role in the exchange of heat, moisture and momentum between them. Its characteristics, including, crucially, its depth, are therefore important parameters in developing the understanding of such exchanges that is needed to get the most out of process studies, parameterisations and climate monitoring [4].

The shallow depth ($\sim$1–3 km), thinness of the top boundary ($\sim$10–100 m) and frequent presence of cloud and rain mean that routine, widely available, accurate and reliable planetary boundary layer height (PBLH) estimates have thus far eluded atmospheric scientists. An intriguing possibility is the use of Radio Occultation measurements, which, on account of their high vertical resolution and relatively uniform spatial distribution (even over oceans) might be thought to have possibilities in this direction. Numerous studies (eg [9], [5], [1]) have confirmed this potential. It was therefore considered time for the ROM SAF to start generating a PBLH product (ROM SAF Product id GRM-26, see [10]), so that its possible utility and reliablity could be assessed by routine monitoring. The natural place to hold the code for such diagnostics is ROPP, another ROM SAF product (ROM SAF Product id GRM-16, see [10]). This report details the algorithms used in ROPP to calculate these diagnostics, together with some preliminary results. Since the details of the algorithms are under discussion and development, these results should not be viewed as the final word on PBLH diagnostics in ROPP.

2 Theory

The top of the planetary boundary layer is characterised by sharp gradients in temperature, humidity and concentrations of tracers. The first two can lead to correspondingly sharp gradients in refractivity and bending angle. A first attempt to diagnose PBLH might therefore simply be to locate the height of maximum (magnitude) of the vertical gradient of a field that is sensitive to these quantities.

But which field should be used? In view of the uncertainty of the usefulness of any of the proposed PBLH diagnostics, it was considered helpful initially to calculate PBLHs based on the profiles of bending angle α, refractivity N and dry temperature T_{dry}, as well as the colocated model temperature T, specific humidity q and relative humidity ρ, if possible. The spread in the various PBLHs should give the user some feeling for the confidence to be assigned to any or all of the PBLHs.

Xie [14] analysed PBLHs calculated for the same six fields. The model fields T, q and ρ were taken from ERA-i reanalyses [11], and the 'observational' data α, N and T_{dry} were simulated ('forward modelled') from these. He found that reliable estimates of PBLH could be obtained by selecting the minima/maxima listed in Table 2.1.

Definitions of PBLH

Field	Name	Method
Bending angle α	PBLH_{α}	Minimum
Refractivity N	PBLH_{N}	Minimum
Dry temperature T_{dry}	$\text{PBLH}_{T\text{dry}}$	Maximum
Temperature T	PBLH_{T}	Maximum
Specific humidity q	PBLH_{q}	Minimum
Relative humidity ρ	PBLH_{ρ}	Minimum

Table 2.1: Definitions of PBLH used in ROPP (after Xie [14]).

Apart from the difference in type of extremum selected for PBLH_{T} and $\text{PBLH}_{T\text{dry}}$ (compared to the other methods), the algorithms for all the PBLHs obey the following pattern. (See the 'ROPP APPS' User Guide IV (at [10]) for more details.)

- Carry out some 'bookwork' to make sure the profiles are ascending, that there are sufficiently many valid data points for ensuing finite difference operations to work, and that essential auxiliary data (eg radius of curvature for bending angles/impact parameters) are available.
- Calculate the geometric height h above the surface of the data points. For N and T_{dry} these are the given refractivity altitudes minus that of the surface geopotential. For T, q and ρ these are the given geopotential heights converted into geometric heights, with the contribution from the surface geopotential again subtracted. For bending angles, which are supplied on impact parameters a, the conversion to geometric height is more complicated, but it has to be done because the contribution to a from the surface refractivity is around 2 km, which is comparable to the PBLH. (Contrast this with the situation for tropopause heights, for which the corresponding shift between impact heights and geometric heights is around 200 m, which is much less significant in a measurement of order 10 km.) For PBLH_{α}, then, the equation $a = rn(r)$ is solved iteratively for $r = h + R_c + u$, where R_c is the radius of curvature, u is the undulation and h is

the required height above the geoid. The refractive index n equals $1+10^{-6}N$ where N is the refractivity, which must therefore be present for this calculation to proceed. $\log N$ is simply interpolated onto the radii at the previous iteration, r^k, in order to calculate the radii at the next iteration via $r^{k+1} = a/n(r^k)$. The height of the surface potential is again subtracted to make the vertical coordinate the height above the surface.

- The valid data are checked to make sure that they start below the lowest possible PBLH (chosen to be 300 m, which should be high enough to avoid surface-layer based inversions [12]), and that they stop above the maximum possible PBLH (chosen to be 5000 m, which is possible over the Sahara on a summer day [7]).

- 1–2–1 smoothing is applied to the dependent variable before calculating the gradients Γ at the halfway points, eg for PBLH_α

$$\Gamma_{i+1/2} := (\partial\alpha/\partial h)_{i+1/2} \approx (\alpha_{i+1} - \alpha_i)/(h_{i+1} - h_i)$$

- The number of local minima (maxima for T and T_{dry}) between 300 m and 5000 m is recorded, and the indices of the strongest two (if possible) are stored[1]. The location of each PBLH is estimated by fitting a quadratic through $(\Gamma_{i*-1/2}, h_{i*-1/2})$, $(\Gamma_{i*+1/2}, h_{i*+1/2})$ and $(\Gamma_{i*+3/2}, h_{i*+3/2})$, where $i*+1/2$ is the index of the local extremum in the vertical gradient Γ. The location of the minimum (maximum for T and T_{dry}) of this quadratic defines the estimated PBLH, as well as the magnitude of the variable (α, say) at the PBLH, which may possibly be of interest.

- The dependent and independent variables at the two strongest possible PBLHs between 300 and 5000 m are stored in the `ROprof` structure.

- If dry temperatures T_{dry} are not available in the dataset then they are estimated from the refractivities N by downwards integration of the defining equation

$$\mathrm{d}\log p/\mathrm{d}z = -\left(g_{\text{wmo}}/R_{\text{dry}}\kappa_1\right) N \exp(-\log p)$$

  (where z is the *geopotential* height, so that we can use constant $g_{\text{wmo}} = 9.80665$ ms^{-2}, $R_{\text{dry}} = 287.05$ J K^{-1} kg^{-1} and $\kappa_1 = 0.776$ K Pa^{-1}) together with a boundary condition provided by a simple climatological estimate of dT_{dry}/dz at the top of the profile. T_{dry} is then simply equal to $\kappa_1 \exp(\log p)/N$.

- Relative humidities are calculated from temperatures, pressures and specific humidities by using the formulas employed in the ECMWF IFS [3]. According to these, the saturated vapour with respect to which ρ is calculated is that over ice if T < 250.16 K, that over water if T > 273.16 K, and a 'quadratic' blend of the two at intermediate temperatures.

- Similarly, if geopotentials are unavailable but are required (ie for PBLH_T, PBLH_q and PBLH_ρ) then, provided the fields are in ECMWF format and the files contain the required A_k and B_k level coefficients, the geopotentials are calculated using the ECMWF IFS formulas [2].

- Various diagnostics, including the number[2] of boundary layers in the profile and the geographical region of the location of the profile (land, subtropical ocean etc) are encoded in a quality control flag, which is also stored in the `ROprof` structure, and thence in the output file.

[1] Discussions with boundary layer experts from the Met Office [7, 8], suggested that two or more 'boundary layers' — that is, regions of different physical characteristics, with sharply marked boundaries between them — would not be unexpected, and that recording the locations of at least the principal two such boundaries could be useful.

[2] Zero, one, two, or more than two.

3 Results

3.1 Overview

Fig 3.1 plots all six PBLHs, and the average of the available ones, for 100 randomly chosen radio occultation measurements from all available missions[1] (and colocated background fields) in April 2013. Several points are immediately clear:

- Only rarely, as in profile A, do the six PBLH estimates exist and agree with each other reasonably closely.
- Very often, there are no observational estimates of PBLH (ie PBLH_α, PBLH_N and $\text{PBLH}_{T_{\text{dry}}}$ are missing). This is because currently only COSMIC observations go below 300 m, the minimum allowed PBLH, below which data must exist for the PBLH search algorithms to begin. (Otherwise one would be finding the minimum or maximum vertical gradient above the lowest observation point — which might be at 3 or 4 km.) Indeed, of the 62 000 observations stored in the Met Office 'MetDB' for April 2013, about 50% were from COSMIC satellites, and about 50% of these occultations failed to penetrate below 300 m, or otherwise failed to generate observational PBLHs, so the overall 'strike rate' for RO-derived PBLHs is currently around 25%. This should improve when Wave Optics processing is introduced into the EUMETSAT processing chain, which should provide useful GRAS bending angles (and refractivities and dry temperatures) down to the surface.
- Even where 'observational' PBLHs exist, they commonly disagree with 'background' PBLHs, eg profile B. (But note that some of these PBLHs agree with the second strongest background PBLH.)
- Often, there is a clear 'odd one out', such as PBLH_T in profile C, which is easily detectable by diagnostics such as those in Fig 3.1 but which might be difficult to treat automatically. The odd one out may in fact turn out to be the correct one.
- Sometimes, as in profiles D and E, there is a wide disparity in the PBLHs. If these result from different features of the boundary layer then simply averaging them may not be a sensible thing to do.
- Rather large PBLHs can occur over land, eg profile F. This is particularly to be expected if, as is the case here, the observation takes place at the end of the day, when a convective boundary layer has had time to build up.

3.2 Selected profiles

We now examine each of the selected occultations in Fig 3.1 in detail.

[1] About 60% COSMIC, 20% Metop, and the rest from GRACE-A, TerraSAR-X and C/NOFS.

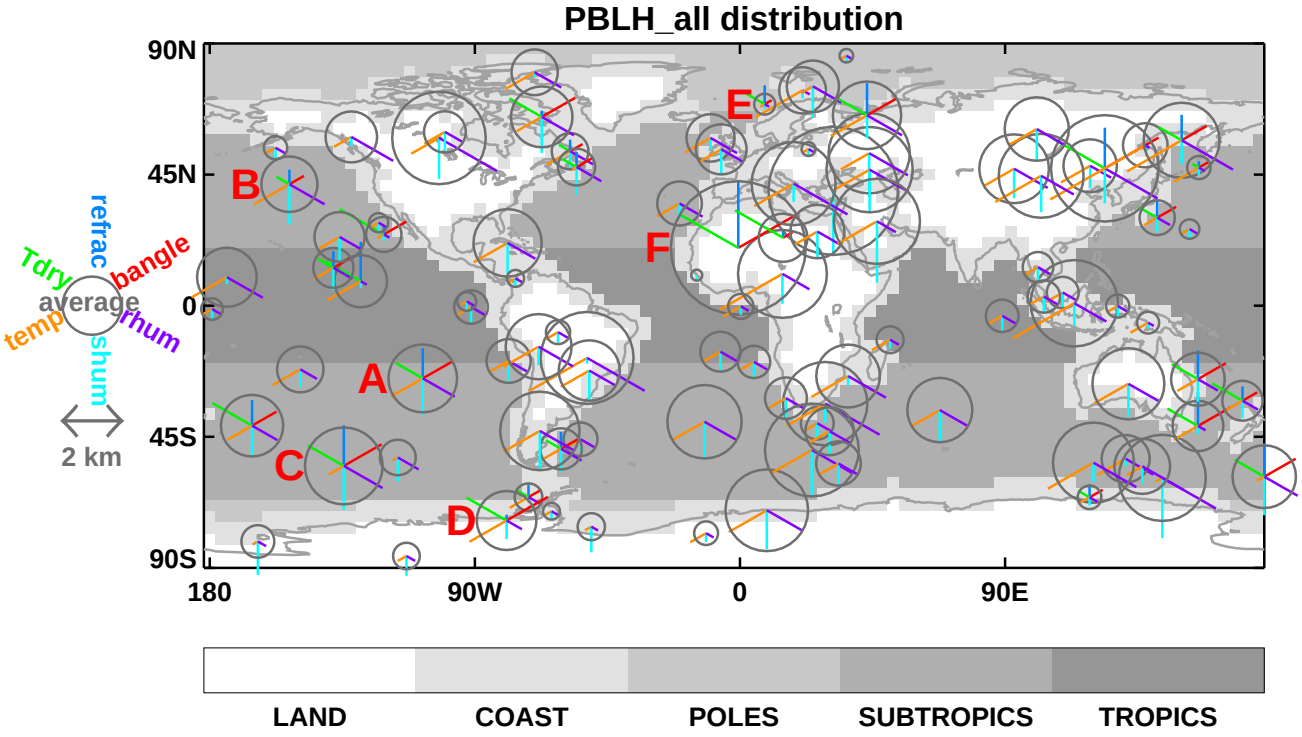

Figure 3.1: 100 example PBL heights, April 2013, from all instruments. PBLH_α, PBLH_N, $\text{PBLH}_{T_{\text{dry}}}$, PBLH_T, PBLH_q, PBLH_ρ all shown (where available), as is their average.

3.2.1 Profile A: Marine stratocumulus region

These regions are characterised by moist boundary layers capped by a sharply defined temperature inversion. If automatic PBLH detection algorithms fail to work here, they are unlikely to work anywhere. Fortunately, they appear to be reasonably reliable in these regions.

Fig 3.2 plots the basic variables (COSMIC-observed bending angle, refractivity and dry temperature; colocated Met Office background temperature, specific humidity and relative humidity) in blue, and their vertical derivatives in red. The minimum or maximum gradient of each defines a PBLH according to Table 2.1. The strongest ones, labelled 'PBLH' in Fig 3.2, are clearly defined and in close agreement at around 2.3 km. But even in this case, the second strongest extrema, labelled 'PBLH2' in Fig 3.2 show marked differences, with the observationally based PBLHs (top row) favouring a second PBLH at about 3.1 km while the model based PBLHs (bottom row) favour a much lower second PBLH at about 0.6 km. These distinctions and inconsistencies are echoed loudly in some of the other profiles.

3.2.2 Profile B: Marine extratropics

We might expect to find a more complicated PBL structure in a region more disturbed by the passage of extratropical highs and lows, and indeed we do: Fig 3.3 shows a clear *double* PBLH, which comprises a low inversion-capped PBL below 1 km, and a higher (cumulus-capped?) inversion above 2.5 km. Apart from PBLH_T, which fails to pick out the lower one, all the diagnostics detect both of these, and they appear to be of similar strength (ie the magnitudes of the maximum/minimum gradients are close) so that the distinction between 'PBLH' and 'PBLH2' is a little dubious. Consideration of profiles like these led us to record (up to) two PBLHs per profile. The loftier of the observational

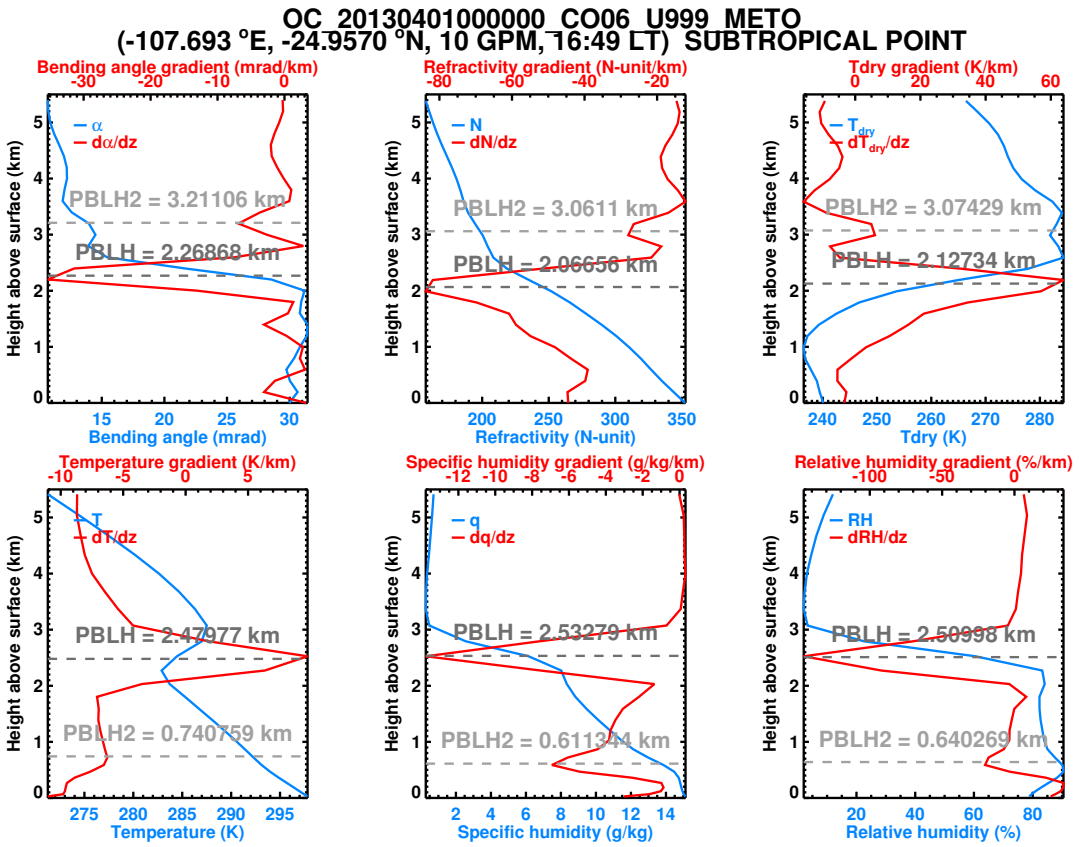

Figure 3.2: PBL derivations for profile A in Fig 3.1. Top row: COSMIC bending-angle-, refractivity- and dry-temperature-based PBLHs; bottom row: Met Office temperature-, specific-humidity and relative-humidity-based PBLHs. Basic fields in blue (lower x-axis); vertical gradients in red (upper x-axis). PBLHs from the first and second strongest minima (or maxima for T_{dry} and T) are both shown.

PBLHs are comparable to the stronger of the model-based PBLHs. For the lower boundary layer, the observational estimates are about twice as large as those from the colocated model profiles. Vertical resolution ($\sim$150–200 m for the observations; $\sim$50–100 m for the model) may be playing a part here.

3.2.3 Profile C: Marine extratropics again

This profile clearly shows (Fig 3.4) another double PBLH. In this case the higher one, at around 2.8–3.0 km is stronger in all cases but PBLH_T, which favours the lower one at around 1.2–1.4 km. Relying on the latter would clearly be a mistake in this case. (It will also be seen that for PBLH_q and PBLH_ρ, the first and second PBLHs are of very similar strength.) This highlights the need to be aware of the likely 'multimodal' PBL structure, which implies that different estimates of the PBLH may result from the detection of *different* features (extrema) in the profile, not just more-or-less accurate estimations of the *same* feature. Recording two PBLHs, and noting whether 0, 1, 2 or more than 2 potential PBLHs are detected, are steps in this direction.

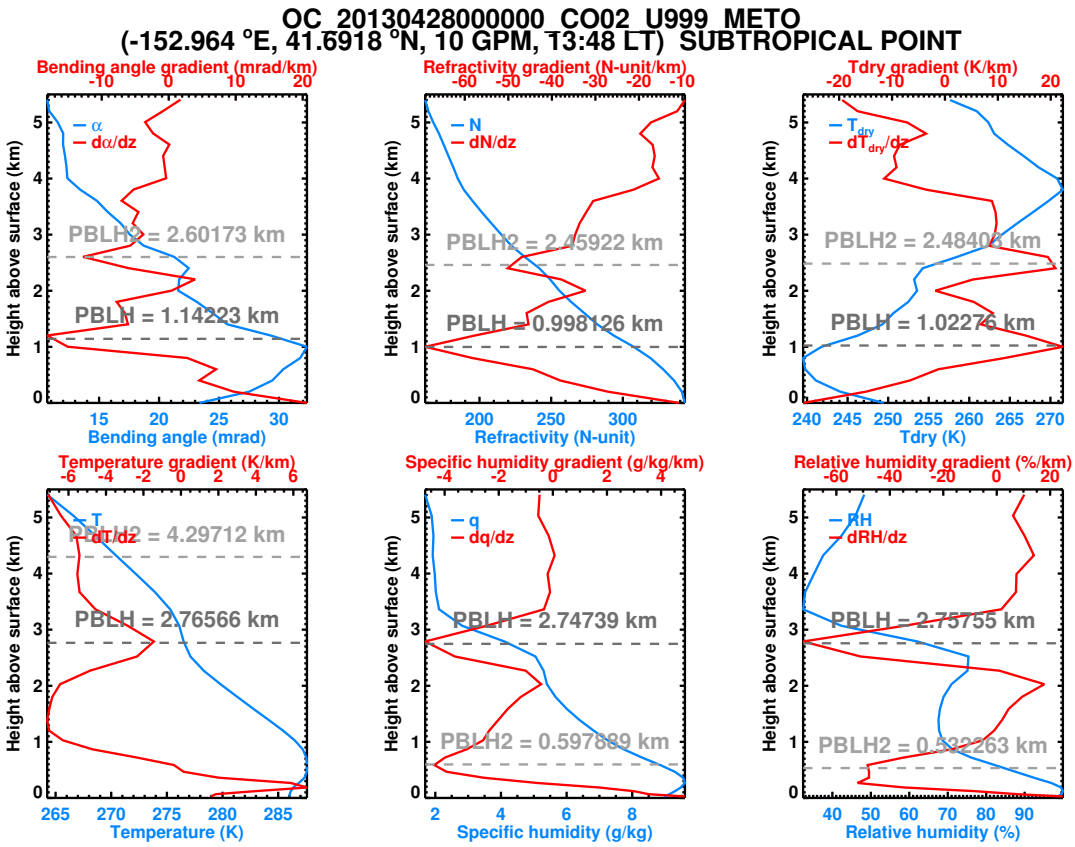

Figure 3.3: As Fig 3.2, except for profile B in Fig 3.1.

3.2.4 Profile D: Antarctic coast

Calculating a boundary layer height over a high (700 m ASL), cold (-15 °C) Antarctic coastal point might be considered a challenge, but the observational PBLH diagnoses all return a PBLH of around 3.1 km, although for PBLH_N this is the second strongest PBLH, the first appearing at 400 m (Fig 3.5). (If this had been a little lower, below 300 m, it would have been excluded from the minimum vertical gradient search region altogether. This is another difficulty in trying to automate the PBLH location algorithms.) The higher PBLH coincides with a region with a slacker temperature lapse rate. The humidity, however, has a minimum lapse rate much lower down, which is why PBLH_q and PBLH_ρ are around 1.2 km. This highlights the need for some physical understanding of the likely structure of the boundary layer at the place/time/season in question, and again cautions against the adoption of a single, automatically derived, PBLH.

3.2.5 Profile E: Polar ocean

Many possible PBLHs appear in this occultation: 2.9 km, 1.5 km, 1.0 km and 0.3 km (see Fig 3.6). The complexity of the profiles suggests that defining the PBLH by the location of an extremum in the vertical derivative of the data may be too simplistic in this situation. Simply averaging the calculated ones would probably not be a good idea.

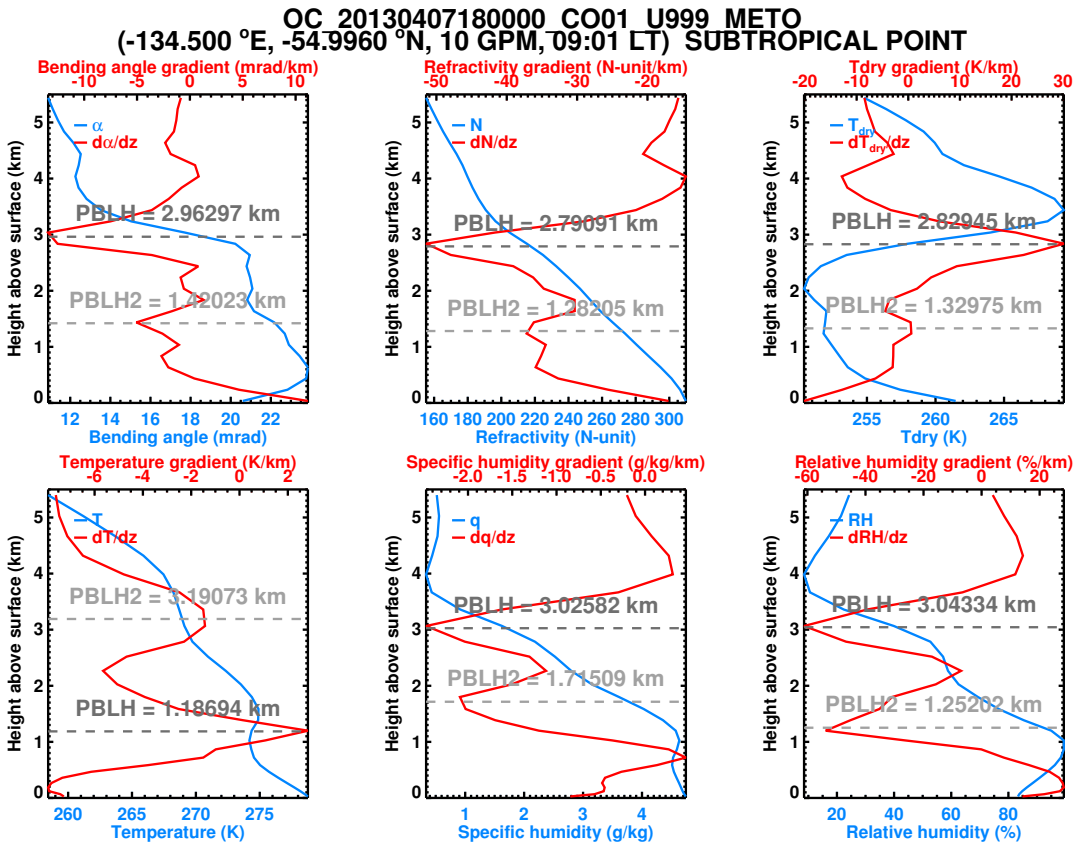

Figure 3.4: As Fig 3.2, except for profile C in Fig 3.1.

3.2.6 Profile F: Sahara desert

At the end of the day (∼1800 LT) over this desert point, a deep, dry, neutrally stable boundary layer of slowly falling specific humidity has built up (see Fig 3.7). Observational measures put its top at around 4.5 km. It seems likely that the corresponding model estimates would be a little higher than 5.0 km. There are therefore, perhaps, grounds for raising the maximum allowed PBLH to (say) 6 km, but if this were done then the difference between the observational and model-based PBLH estimates would be at least 0.5 km, which probably raises as many questions as it answers.

Once again, this example shows the wide range of PBLHs that can be produced by naively defining it as the location of an extremum of the vertical derivative.

3.3 Systematic analysis

It seems clear from the examples in Secs 3.1 and 3.2 that, at present, there is too much uncertainty and variability in any measure of PBLH to suggest that it be assimilated into an NWP model, even if the procedure to do so were clear. There remains, however, the possibility that a suitably averaged PBLH could be useful validation dataset for atmospheric process studies or, eventually perhaps, climate monitoring and/or modelling. This Section therefore considers the average properties of the PBLHs diagnosed from the 62 000 radio occultation measurements in the Met Office observational database ('MetDB') in April 2013. About 55% of these occultations are from the COSMIC mission, 25% from Metop, 10% from TerraSAR-X, 5% from GRACE-A and 5% from C/NOFS.

A useful climatology of PBLH has been generated by von Engeln and Teixeira [13], who defined the

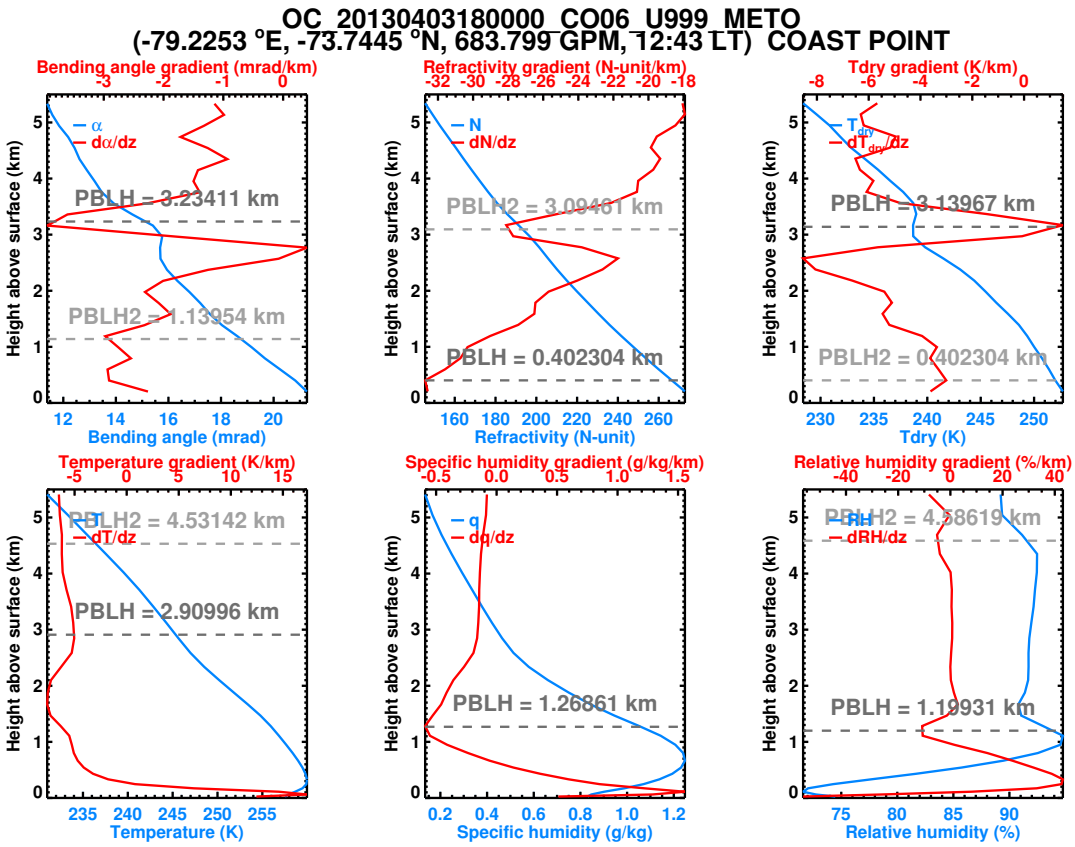

Figure 3.5: As Fig 3.2, except for profile D in Fig 3.1.

PBLH as the location of the minimum vertical gradient of relative humidity, as derived from 20 years of data from the ECMWF Interim Re-Analysis (ERA-Interim, [11]). Their mean $PBLH_\rho$ for March-April-May is shown in Fig 3.8. The key features are:

1. There are consistently low (< 1 km) PBLHs in the oceans along the western coasts of the continents, where upwelling cold waters suppress convection in the boundary layer;
2. West of these narrow ribbons lie the broad marine stratocumulus regions, where boundary layer convection consistently develops over warmer waters until it is capped by a temperature inversion somewhere between 1.5 and 2.0 km above sea level;
3. There are low PBLHs over the tropical rainforests, presumably resulting from the small distance that a moist air parcel would need to ascend before becoming saturated;
4. For the opposite reason there are large PBLHs over desert regions, particularly between 1200 LT and 1800 LT (time-dependence not shown);
5. The PBLHs over cold land (Antarctic and Greenland) are generally below 0.5 km; and
6. The PBLHs over cold water (Arctic ocean) are generally around 1.0 km.

Although these are average features derived from 20 years of model relative humidity data, and for three months rather than one, it is useful to compare Fig 3.8 to the corresponding PBLHs for April 2013, derived according to the theory described in Sec 2. We treat each PBLH in turn.

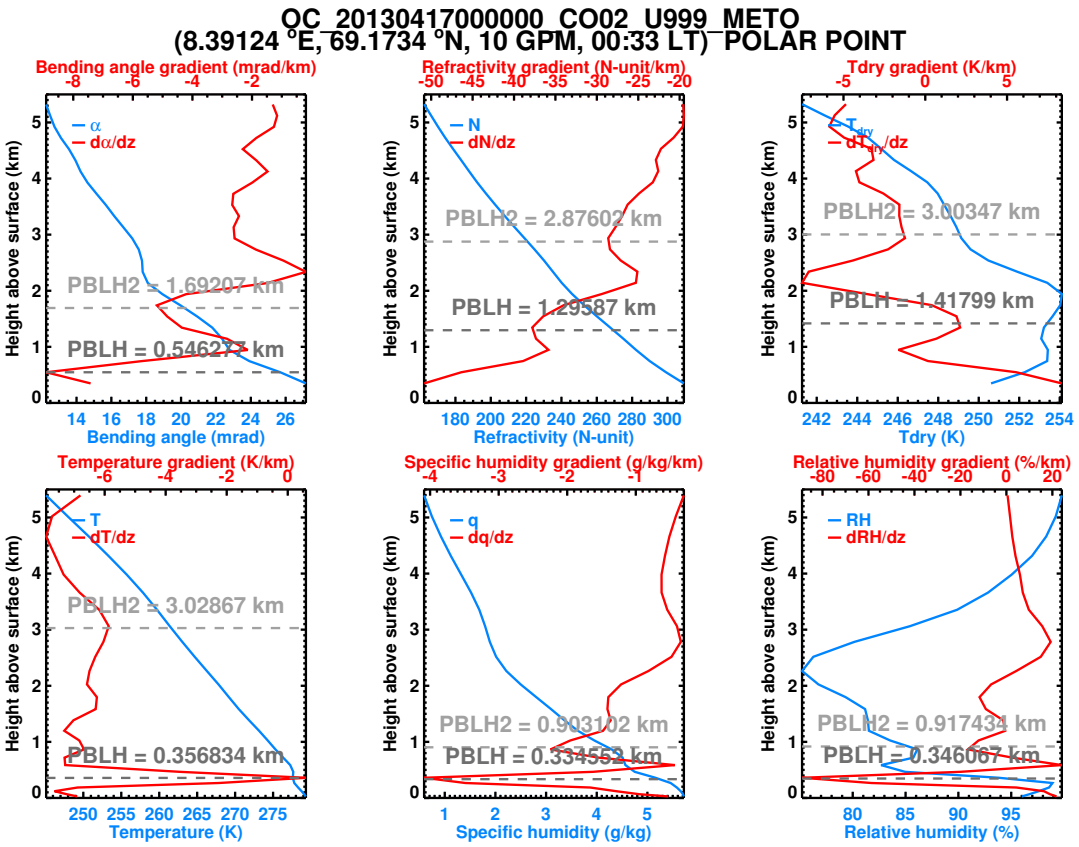

Figure 3.6: As Fig 3.2, except for profile E in Fig 3.1.

3.3.1 Bending angle, PBLH$_\alpha$

Fig 3.9 shows the average PBLH of the 26% of the 62 000 profiles in April 2013 for which it is calculable (all of which are COSMIC). These have binned on a 4°×4° grid, which means there are on average about 4 occultations per gridcell, although these are concentrated in the extratropics, say 30° < |latitude| <75°. (The data have also been smoothed 1–2–1 in both directions.) One can see that the *pattern* of PBLH$_\alpha$ mirrors the key aspects of von Engeln and Teixeira's climatology discussed above: the low values just off the western boundaries of the continents, the high values over the continental interiors (except for Antartica and Greenland), etc. But the overwhelming conclusion is that the bending-angle-based PBLHs are too high, perhaps by as much as 500 m. This clearly needs to be investigated.

3.3.2 Refractivity, PBLH$_N$

This (Fig 3.10) is clearly rather closer to von Engeln and Teixeira's climatology shown in Fig 3.8. In particular, there are none of the unrealistically large (> 3 km) values over the tropical sea that spoil the PBLH$_\alpha$ map in Fig 3.9. On the other hand, the small PBLHs over Antarctica are not estimated accurately. Overall, the average PBLH$_N$ is about 300 m smaller than that of PBLH$_\alpha$.

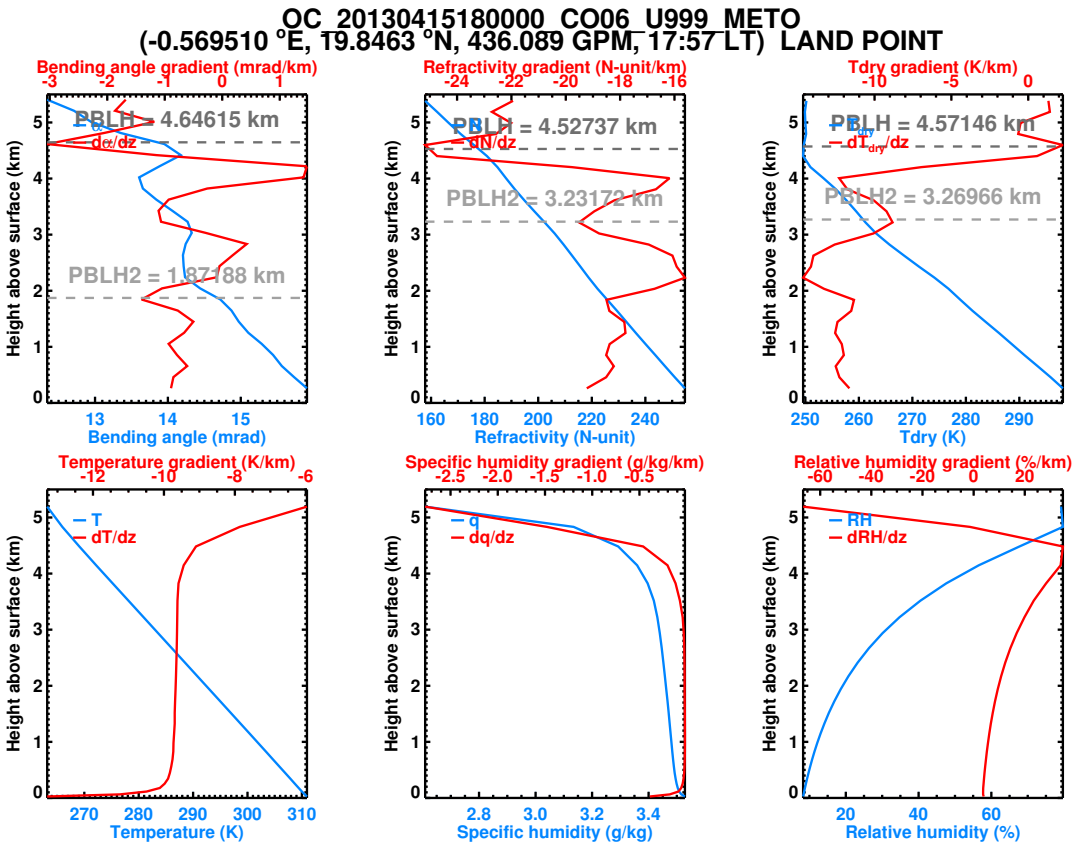

Figure 3.7: As Fig 3.2, except for profile F in Fig 3.1.

3.3.3 Dry temperature, PBLH$_{T_{\mathrm{dry}}}$

The dry temperature-based PBLH in Fig 3.11 is excessively large everywhere, with a mean value over 300 m higher than even that of PBLH$_\alpha$. It would therefore appear to be of little value in its current form.

Note, however, that if we use the *lower* of the two strongest possible PBLHs, rather than the *stronger* of the two (see Fig 3.12), then things are much closer to the climatology of Fig 3.8, although there are still excessively large values over the tropical ocean, and continental land values are (understandably) underplayed. But the difference between Figs 3.11 and 3.12 shows that there might be some mileage in combining the two PBLHs, perhaps according to the location/season/time of day, in order to get the best possible estimate of PBLH from dry temperature.

3.3.4 Temperature, PBLH$_T$

The gridded PBLH based on colocated background profiles from the Met Office 70L operational NWP model is shown in Fig 3.13. Patterns over the ocean are much closer to the climatology of Fig 3.8 — in particular, the low marine PBLHs off the west coasts of the continents are much better established, as are the higher PBLHs in the marine stratocumulus regions further west. And it is the only PBLH estimate yet that captures the reduced PBLH over the ocean in the deep tropics. The values over land, however, are not so good: the low values over the tropical rainforests are entirely absent, presumably because the diagnostic takes no account of the moisture that determines the cloud base in these regions, and the values over Antarctica and Greenland are also too large.

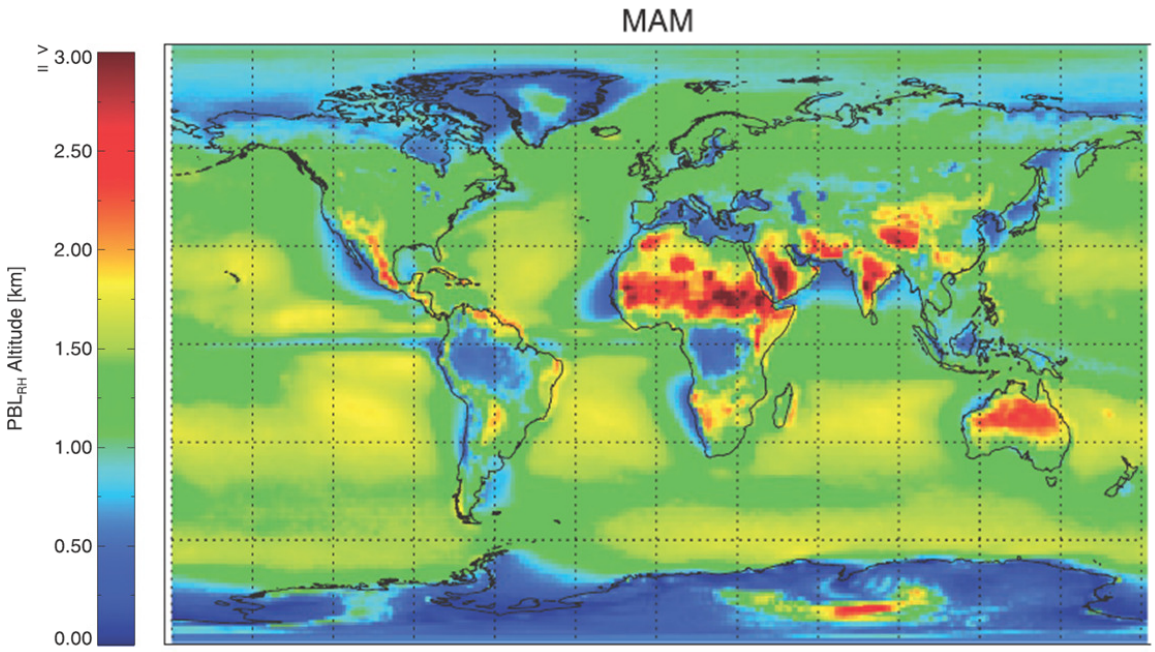

Figure 3.8: Climatological PBLH$_\rho$ derived by von Engeln and Teixeira [13] from 20 years of ERA-i data.

Note that the model-based PBLH diagnostics PBLH$_T$, PBLH$_q$ and PBLH$_\rho$ are derived from much larger samples than their observational equivalents PBLH$_\alpha$, PBLH$_N$ and PBLH$_{T_{\text{dry}}}$. For instance, over 95% of the 62 000 occultations in April 2013 generate 'valid' PBLH$_T$s.

3.3.5 Specific humidity, PBLH$_q$

The background specific-humidity-based PBLH estimate shown in Fig 3.14 is very close to von Engeln and Teixeira's climatology (Fig 3.8). It nicely captures the low PBLHs over the tropical oceans, and the tropical rainforests. Antarctic values are still a little high, however.

3.3.6 Relative humidity, PBLH$_\rho$

Interestingly — since the relative-humidity-based PBLH is based on the same criterion as von Engeln and Teixeira's climatology (namely, the location of the minimum of $\partial\rho/\partial h$) — the map of the PBLH$_\rho$ shown in Fig 3.15 is more different to the climatology than that of PBLH$_q$ (see Fig 3.14). Overall, it looks very similar to PBLH$_T$ (Fig 3.15). Values are too large generally, except off the western coasts of the continents, where the low PBLHs are reasonably well captured.

3.3.7 Average, PBLH$_{av}$

For the record, we show the average of the available PBLH diagnostics in Fig 3.16. Encouragingly, yhe pattern is reasonably close to that of the climatology of Fig 3.8, but the PBLHs are too high over the ITCZ, the tropical rainforests and Antarctica. Evidently these failings are inherited from those of the components of the average, principally PBLH$_\alpha$, PBLH$_{T_{\text{dry}}}$ and PBLH$_T$. PBLH$_{av}$ is closest, in a least squared difference sense, to PBLH$_T$ and PBLH$_\rho$.

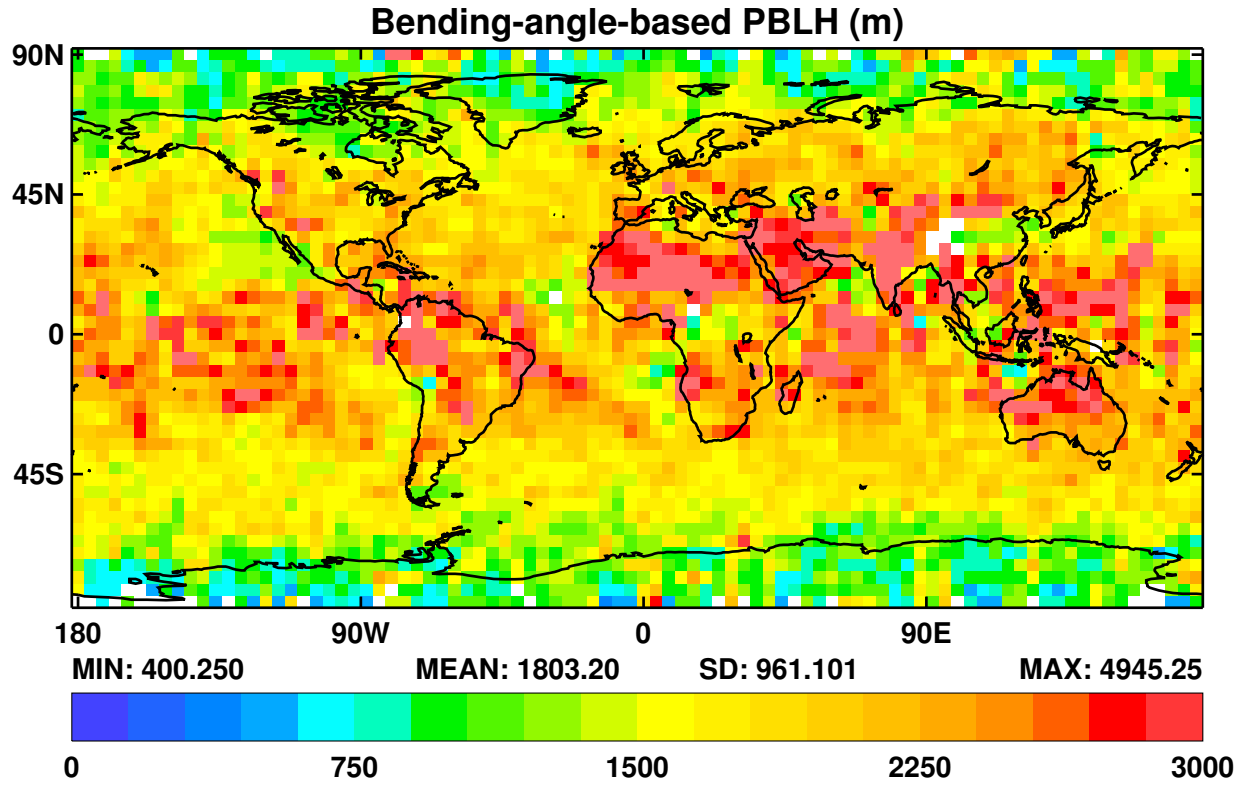

Figure 3.9: PBLH$_\alpha$ derived from all (COSMIC) observations in April 2013, gridded at 4° resolution, smoothed 1–2–1 in both directions.

3.4 Comparison of the various PBLH schemes

3.4.1 Height of PBLs

Table 3.1 lists the global mean values of PBLH$_\alpha$, PBLH$_N$, PBLH$_{T_{\text{dry}}}$, PBLH$_T$, PBLH$_q$ and PBLH$_\rho$, as well as the average of all of those that are available, PBLH$_{av}$. We record the mean of the *strongest* PBLH (ie the one with the largest absolute magnitude of vertical gradient), the mean of the *second strongest* PBLH, the mean of the higher of the two (if both are available, otherwise just the available one) and the mean of the lower of the two (if both are available, otherwise just the available one).

Global mean PBLHs (km)							
Nature	PBLH$_\alpha$	PBLH$_N$	PBLH$_{T_{\text{dry}}}$	PBLH$_T$	PBLH$_q$	PBLH$_\rho$	PBLH$_{av}$
Strongest	1.8	1.5	2.1	1.7	1.4	1.9	1.7
Second strongest	2.3	2.1	2.6	2.5	2.2	2.4	2.4
Higher	2.8	2.5	3.1	2.9	2.5	3.0	2.8
Lower	1.3	1.1	1.5	1.4	1.1	1.3	1.2

Table 3.1: Global mean PBLHs calculated from (COSMIC) observations in April 2013, and the colocated Met Office background fields.

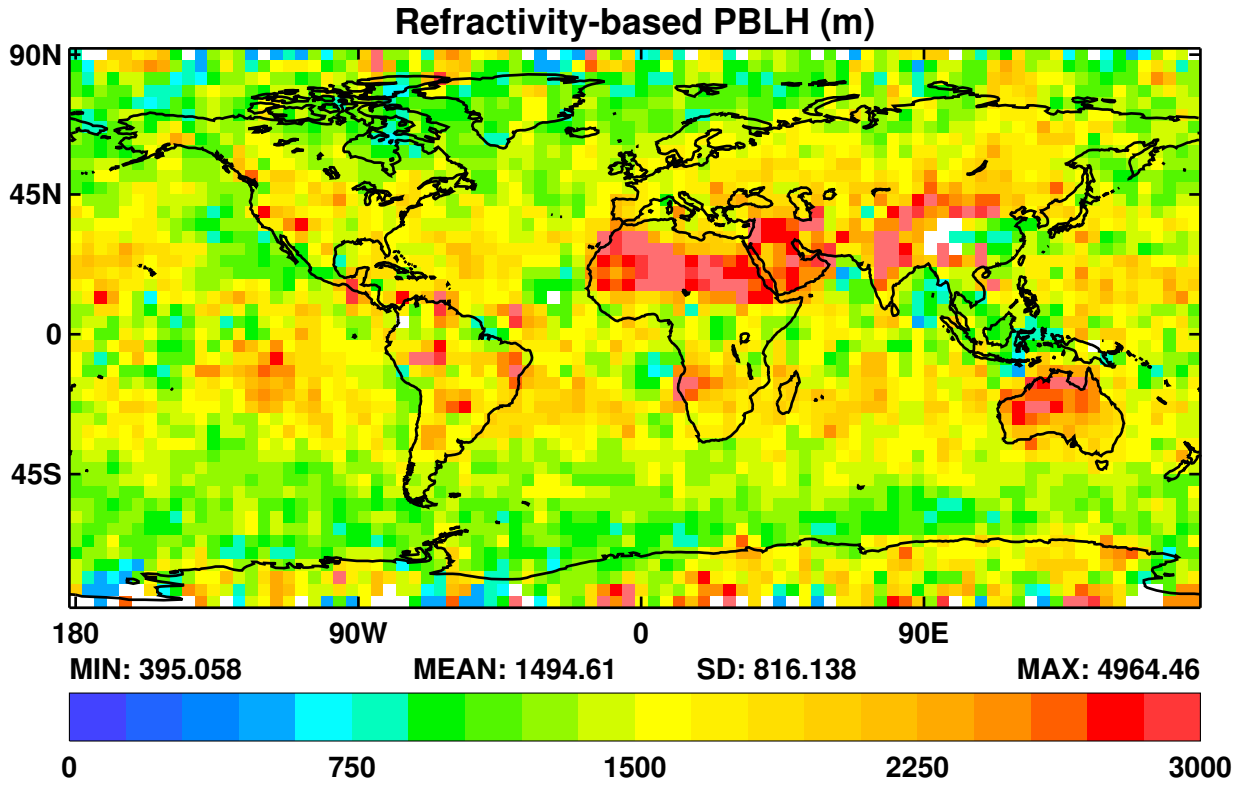

Figure 3.10: PBLH$_N$ derived from all (COSMIC) observations in April 2013, gridded at 4° resolution, smoothed 1–2–1 in both directions.

It is clear from Table 3.1 and the analysis of Sec 3.3 that:

- The stronger of the two principal PBLHs is generally lower than the second strongest.
- The closest observationally based estimate of PBLH to the ERA-interim climatology is that derived from refractivity, PBLH$_N$, which has a global average value of about 1.5 km. The PBLH based on the lower of the two PBLH$_{T_{\text{dry}}}$ would work reasonably well if refractivity were not available.
- The best model-based estimate of PBLH is PBLH$_q$, which has an average value of about 1.4 km.

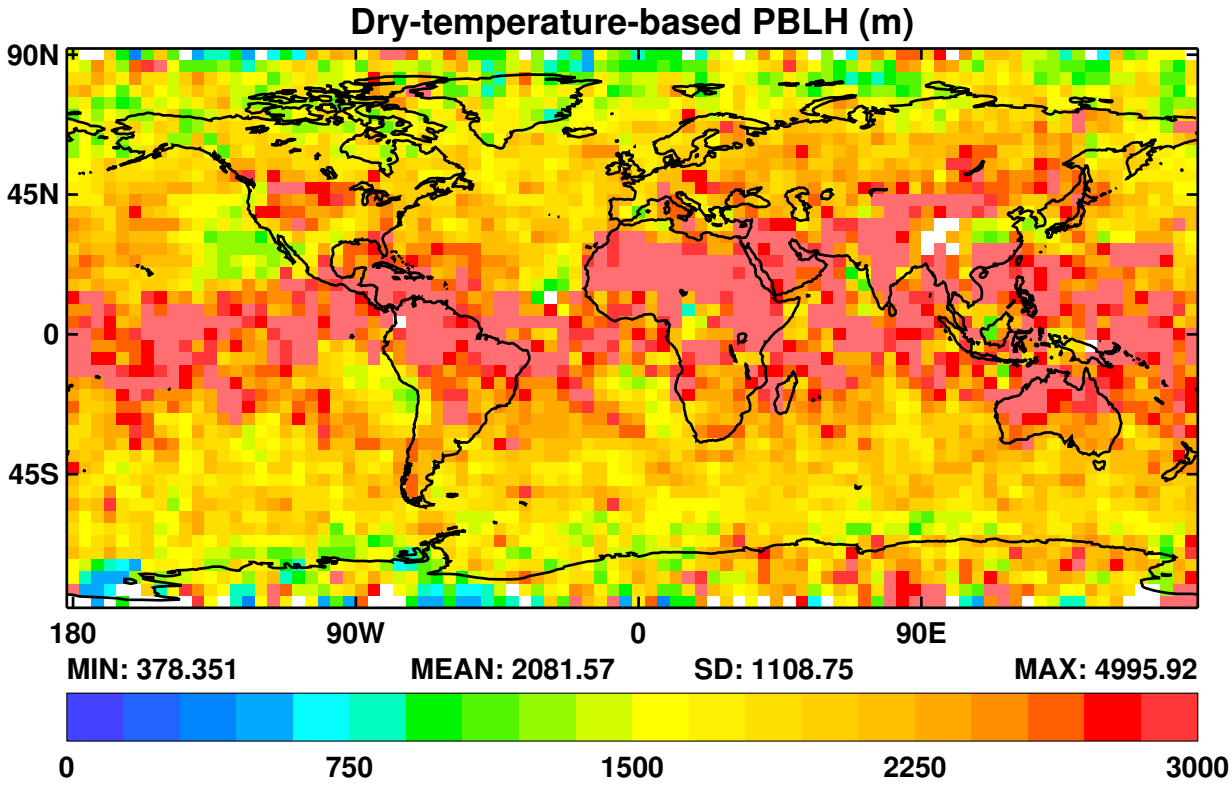

Figure 3.11: $\mathrm{PBLH}_{T_{\mathrm{dry}}}$ derived from all (COSMIC) observations in April 2013, gridded at 4° resolution, smoothed 1–2–1 in both directions.

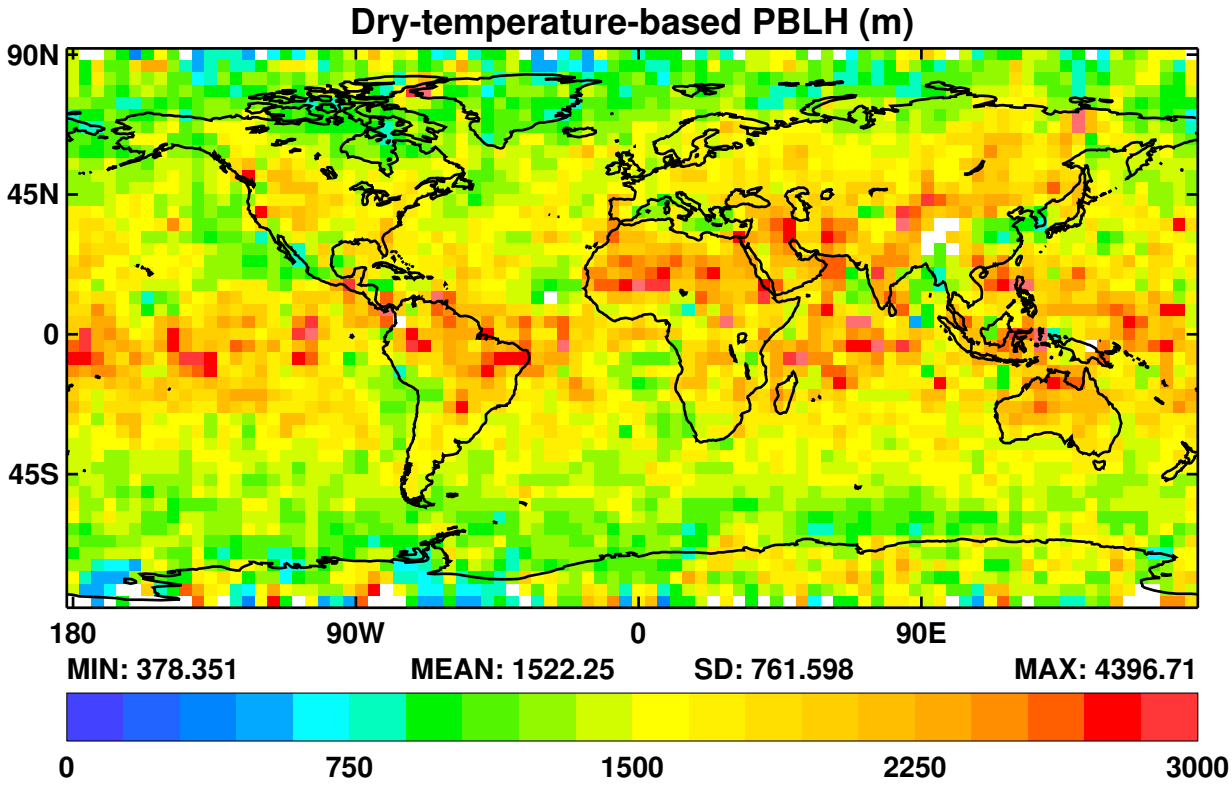

Figure 3.12: *Lower* $\mathrm{PBLH}_{T_{\mathrm{dry}}}$ derived from all (COSMIC) observations in April 2013, gridded at 4° resolution, smoothed 1–2–1 in both directions.

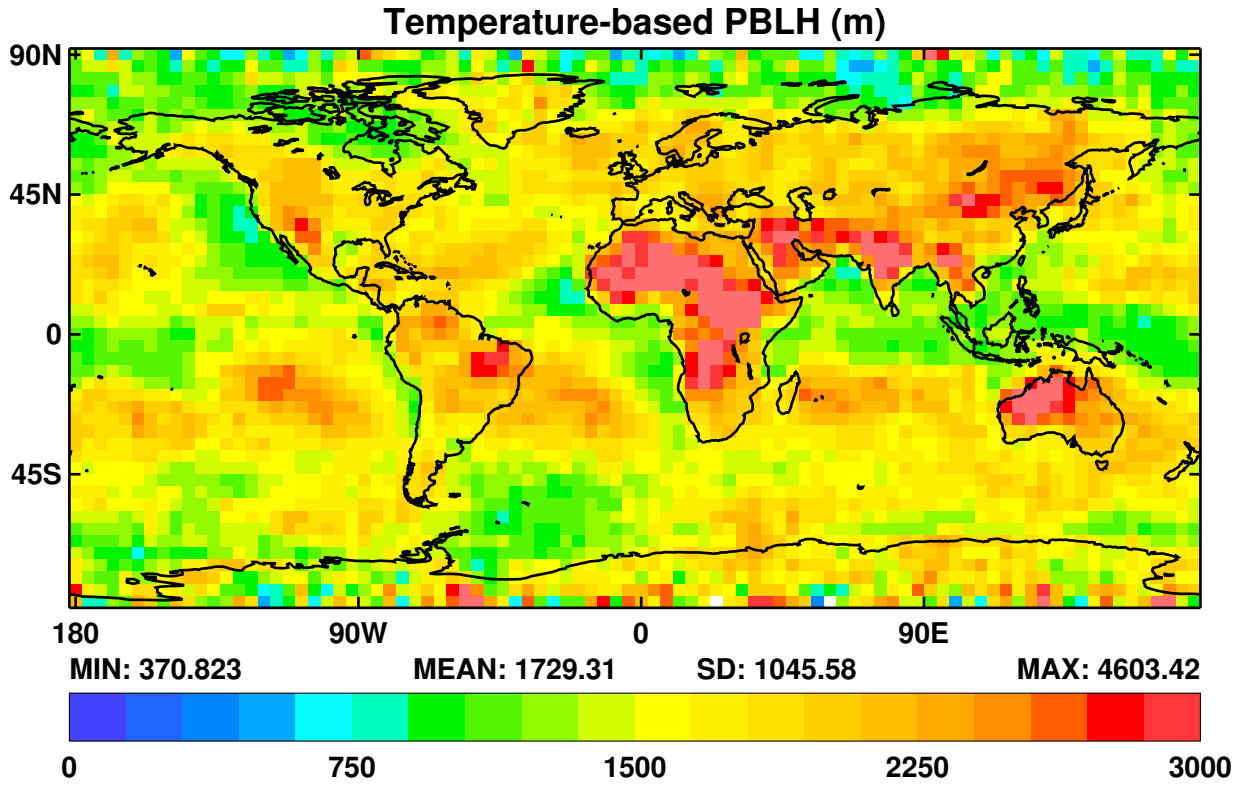

Figure 3.13: PBLH$_T$ derived from Met Office backgrounds in April 2013, gridded at 4° resolution, smoothed 1–2–1 in both directions.

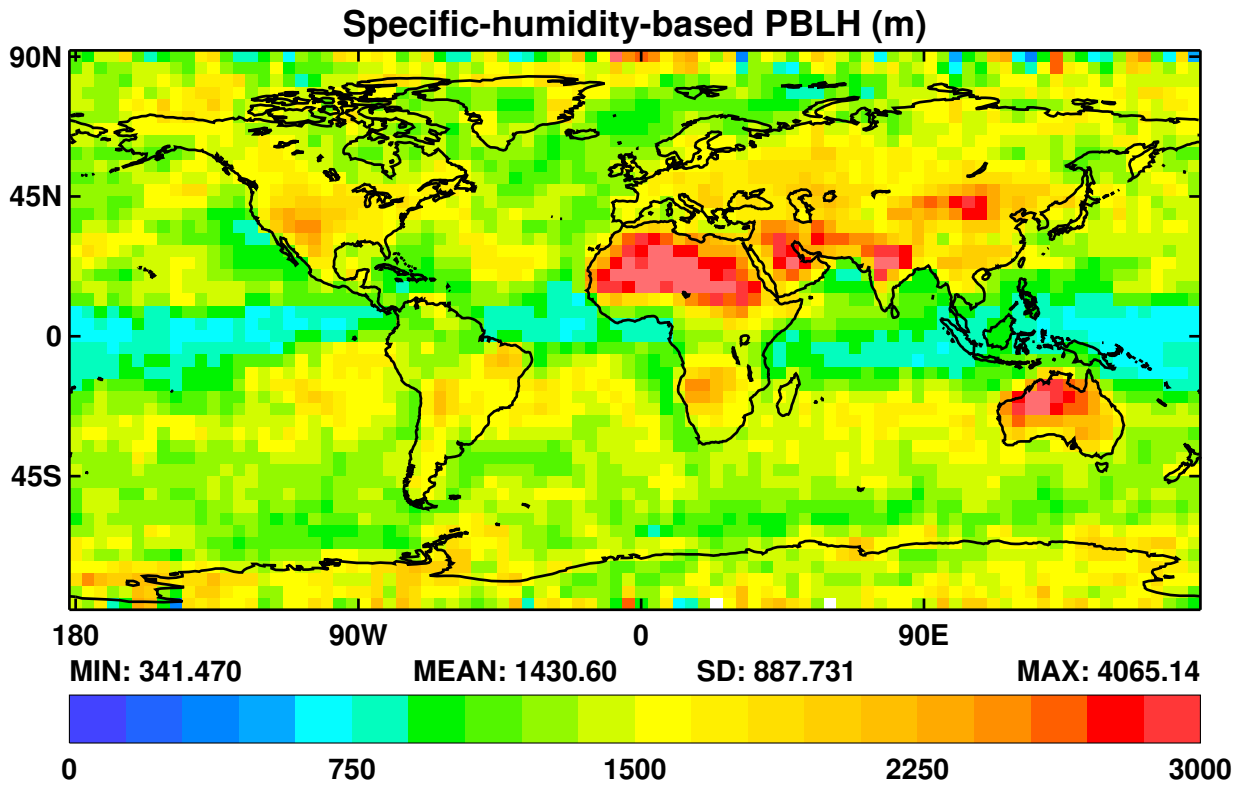

Figure 3.14: PBLH$_q$ derived from Met Office backgrounds in April 2013, gridded at 4° resolution, smoothed 1–2–1 in both directions.

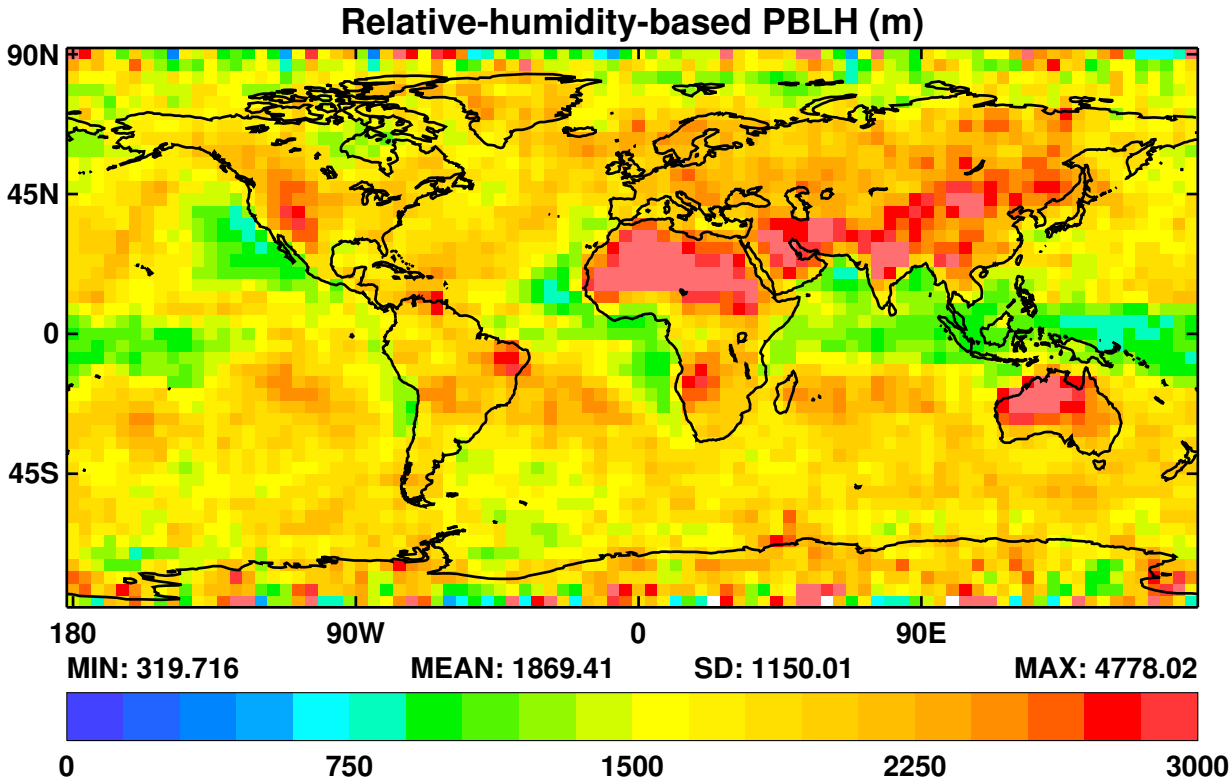

Figure 3.15: PBLH$_\rho$ derived from Met Office backgrounds in April 2013, gridded at 4° resolution, smoothed 1–2–1 in both directions.

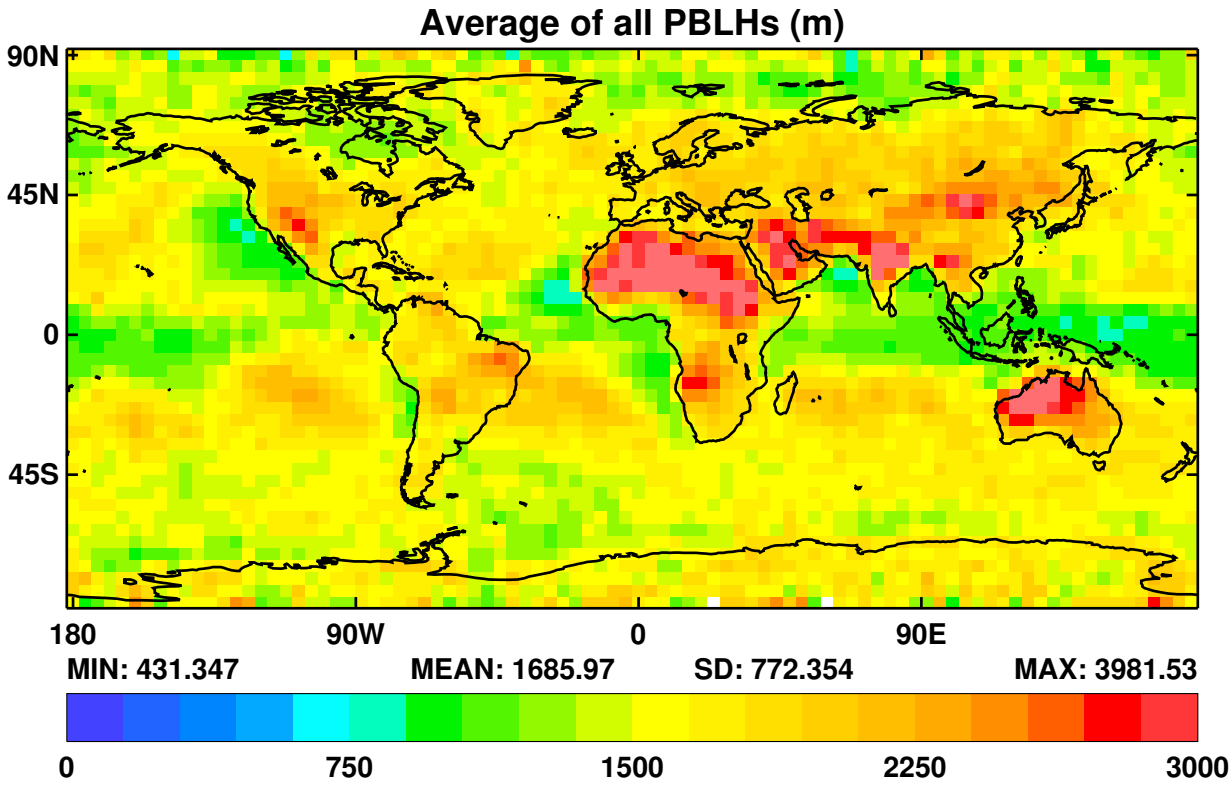

Figure 3.16: Average of all PBLHs derived from all (COSMIC) observations and Met Office backgrounds in April 2013, gridded at 4° resolution, smoothed 1–2–1 in both directions.

3.4.2 Number of PBLs

Table 3.2 shows the frequency with which zero, one, two or more than two PBLHs are diagnosed, for each of the variables.

Distribution of the number of possible PBLHs (%)						
No. of PBLHs	$PBLH_{\alpha}$	$PBLH_{N}$	$PBLH_{T_{dry}}$	$PBLH_{T}$	$PBLH_{q}$	$PBLH_{\rho}$
Zero	74.4	74.6	74.5	1.2	0.0	1.2
One	0.0	0.3	0.0	6.2	3.8	3.7
Two	0.1	1.7	0.7	26.3	22.9	20.5
More than two	25.5	23.4	24.8	66.3	73.3	74.6

Table 3.2: Frequencies of possible PBLHs for COSMIC occultations / colocated Met Office backgrounds in April 2013.

From this it is clear that:

- As noted before, only about a quarter of the profiles generate an observationally based PBLH estimate;
- A single local minimum/maximum in the vertical gradient of a variable between 300 m and 5000 m is rare (<5% frequency of occurrence);
- If at least one PBLH can be identified, the likelihood is that more than two can be so identified.

3.5 Bending angles from forward modelled background fields

In view of the clear differences in the profiles and global PBLH maps between the observational fields (α, N and T_{dry}) and the background model fields (T, q and ρ) shown in the previous Sections, it is natural to analyse the PBLHs derived from simulated observations, which are derived by 'forward modelling' those background fields. Such a procedure should help to factor out effects arising from the different vertical resolutions of the two types of profile, uncertainties in the observations (which are replaced by forward modelled uncertainties in the backgrounds), and infelicities in the radio occultation processing (either geometrical optics or wave optics) that generated the 'observed' bending angles.

The PBLHs derived from the forward modelled background fields used above (Met Office 70 level model, profiles colocated with the 62 000 radio occultation measurements during April 2013) have therefore been calculated. (The forward modelled background fields themselves have already been generated by the Met Office Observations Processing System (OPS) from whose archive they were extracted.) The following Sections briefly describe the results, focusing on the differences from the 'true' observational PBLHs described above.

3.5.1 Bending angle, PBLH$_\alpha$

Without exception, the forward modelled bending angles either fail to exist (because, for example, the specific humidity is missing), or, much more often, fail to start below the minimum starting height of 300 m. This is probably because the forward model rules prevents the calculation of bending angles in ducting or super-refracting regions, where the vertical refractivity gradients are strong — at the bottom of the profile. There are therefore no PBLH$_\alpha$ derived from forward modelled background fields.

3.5.2 Refractivity, PBLH$_N$

Generally speaking, the forward modelled refractivities have better defined PBLHs than their observational counterparts. This is presumably because the model source data are inherently smoother than the observations, because both have the same vertical resolution, namely 247 levels with an average spacing of around 200 m. Consider, for example, the 'canonical example', occultation A in Fig 3.1, whose profiles were shown in Fig 3.2. This figure should be compared to that of the forward modelled background fields, as shown in Fig 3.17. It will be seen that the forward modelled PBLHs are (understandably) rather closer to their background sources, at around 2.5 km, than to the observations. In addition, the *second* strongest PBLH is at around 700 m, rather than about 3.1 km in the observations.

The same sharpening of the PBLH is true of profiles B–F in Fig 3.1 too. The key differences from the observational PBLHs are:

- For profile B (N Pacific) all five available profiles show a 'double' PBLH at about 2.7 km and 0.6 km. PBLH$_N$ says the lower is the stronger, while the other four favour the higher of the two.
- In the S Pacific (profile C), PBLH$_N$ now matches PBLH$_T$ ($\sim$ 1.2 km) while the other three measures put the PBLH at about 3.0 km. The second strongest PBLH$_N$ and PBLH$_T$ are at this higher level (while the weaker of the other three are at about 1.2–1.7 km).
- For profile D (Antarctic coast), PBLH$_N$ and PBLH$_{T_{\text{dry}}}$ now match PBLH$_q$ and PBLH$_\rho$ at about 1.1 km. PBLH$_T$ is now the outlier at 2.9 km.

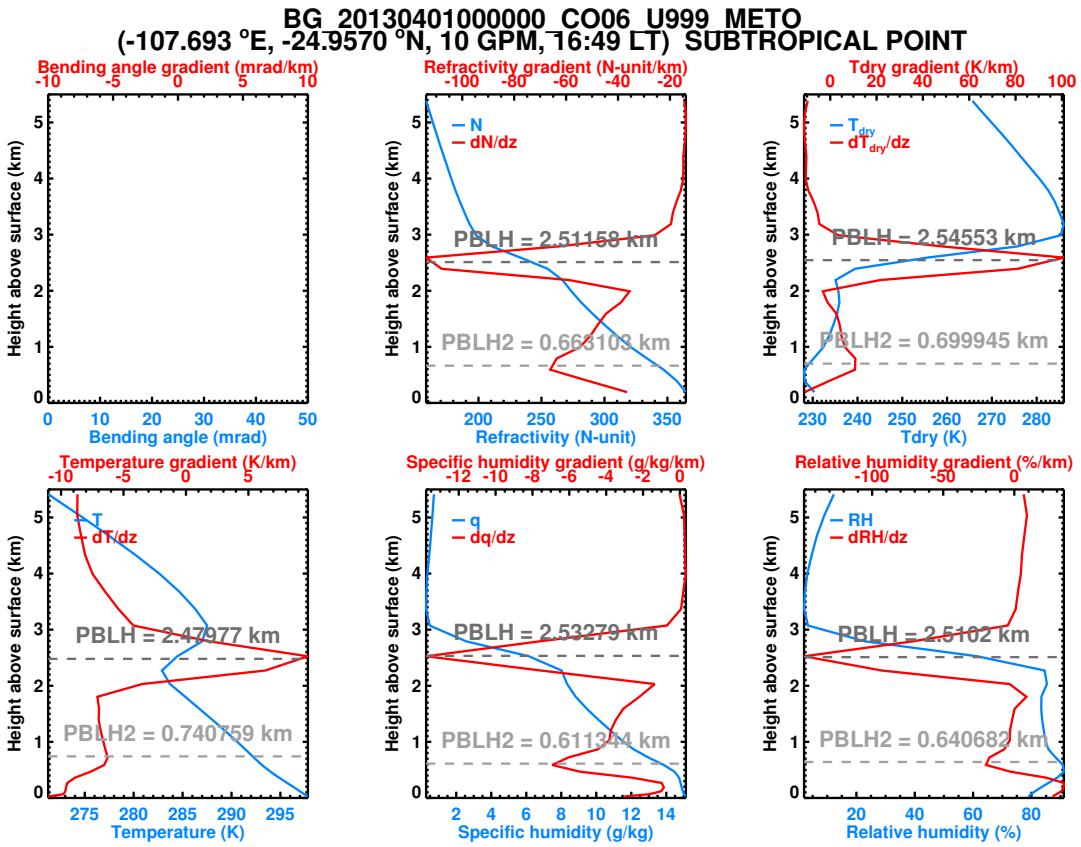

Figure 3.17: As Fig 3.2, except that the top row uses *forward modelled* bending-angle-, refractivity- and dry-temperature-based PBLHs, rather than observed ones.

- In the Arctic (profile E), PBLH_N and $\text{PBLH}_{T_{\text{dry}}}$ are about 0.9 km: closer than the observational PBLHs ($\sim$ 1.3 km) to the model background of 0.35 km.
- For profile F (Sahara), PBLH_N is about 3.5 km, while $\text{PBLH}_{T_{\text{dry}}}$ is about 0.5 km. (The latter comes from a very weak local maximum.) Neither is therefore very close to the 4.5 km derived from profiles of the observations.

This similarity between the PBLHs derived from forward modelled backgrounds and directly from the backgrounds also holds globally. For instance, compare the global mean forward modelled PBLH_N shown in Fig 3.18 with the observational equivalent shown in Fig 3.10. The former is about 100 m lower on average, which is a good thing according to the climatology shown in Fig 3.8, as is the reduction in the deep tropics. The values over dry land, especially Antarctica, are larger and a little more extensive. The high values over Antarctica come about because the background refractivities, largely being only a function of the relatively smooth background temperatures in such dry air, fail to have any local extrema in their vertical gradients from which a PBLH could be identified. Instead, PBLH_N and $\text{PBLH}_{T_{\text{dry}}}$ are drawn to the much less ambiguous turnaround in temperature about 5 km above ground level, ie about 8 km above sea level — in other words, at the Antarctic *tropopause*. (For the temperatures themselves, this turnaround tends to take place just above 5 km AGL, and is therefore not considered a valid PBLH, which is why the PBLH_T in Fig 3.13 fails to display the high values over Antarctica shown in Fig 3.18.) (This is a reason for allowing the maximum allowable PBLH to vary with surface height, at least where the tropopause is low. Until this is done, it is perhaps best to ignore Antarctic PBLHs.)

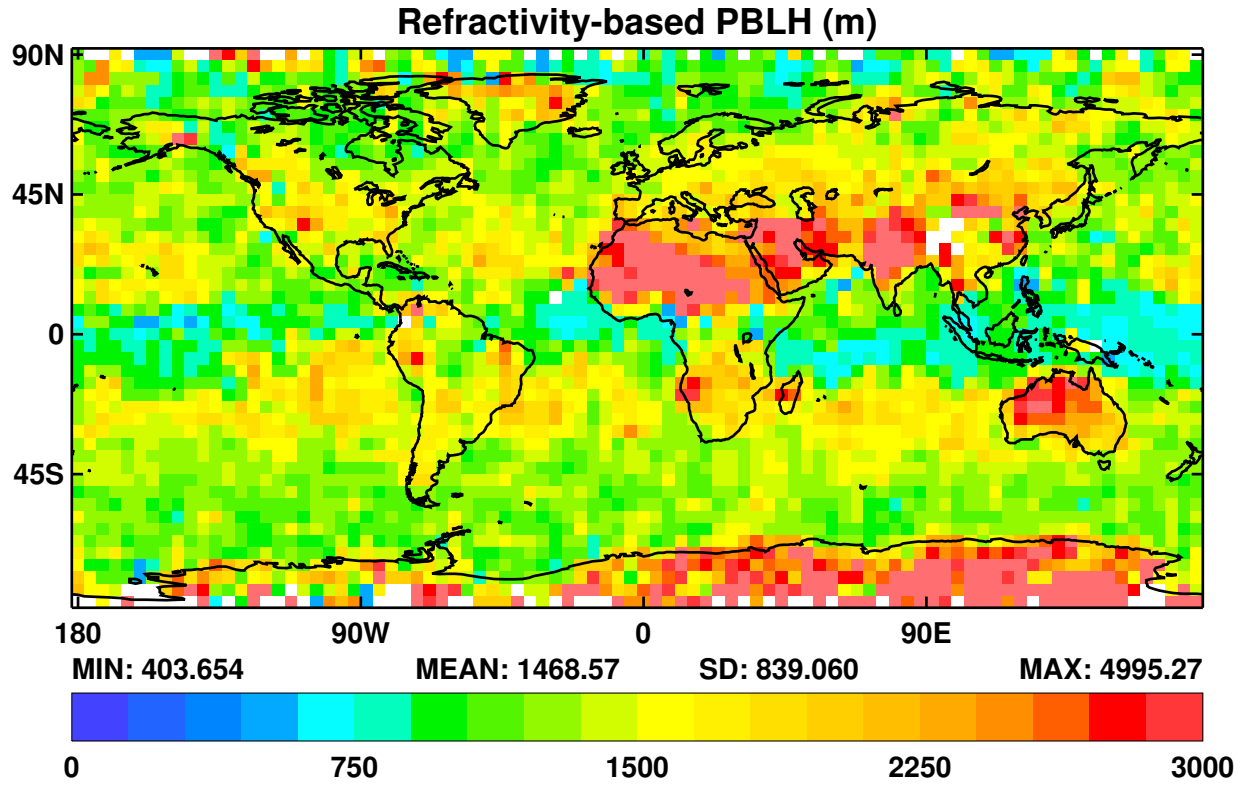

Figure 3.18: PBLH$_N$ derived from forward modelled Met Office backgrounds in April 2013, gridded at 4° resolution, smoothed 1–2–1 in both directions.

3.5.3 Dry temperature, PBLH$_{T_{\text{dry}}}$

The forward modelled PBLH$_{T_{\text{dry}}}$ is very similar to PBLH$_N$, as already exemplified by Fig 3.17. This causes the global mean PBLH$_{T_{\text{dry}}}$, shown in Fig 3.19, to be rather closer to the climatology than its observational equivalent shown in Fig 3.11. In particular, the very high (> 3 km) PBLHs on the equator in the latter have largely disappeared. It is over 400 m smaller on average, which makes it much less of an outlier. For the record, the *lower* PBLH$_{T_{\text{dry}}}$ (not shown) is now probably a little too low, having an average of only about 1400 m, and without much contrast betwen the land and the sea.

3.5.4 Comparison of the various PBLH schemes

We repeat the analysis of Sec 3.4.1 for the forward modelled PBLHs. The results are shown in Table 3.3. Comparison with Table 3.1 shows that the average values of the forward modelled and the observational PBLH$_N$s are rather similar, while the forward modelled PBLH$_{T_{\text{dry}}}$s are slightly ($\sim$ 100–200 m) lower than their observational couterparts.

We also repeat the 'number of PBLHs per profile' analysis of Sec 3.4.2 for the forward modelled PBLHs. The results are shown in Table 3.4. Apart from the absence of PBLH$_\alpha$ there is little significant difference in the distribution of the various types of PBLH (because most of the refractivity altitudes still start several hundred metres above the minimum threshold of 300 m, and are therefore ruled out of the calculation of PBLH$_N$ or PBLH$_{T_{\text{dry}}}$).

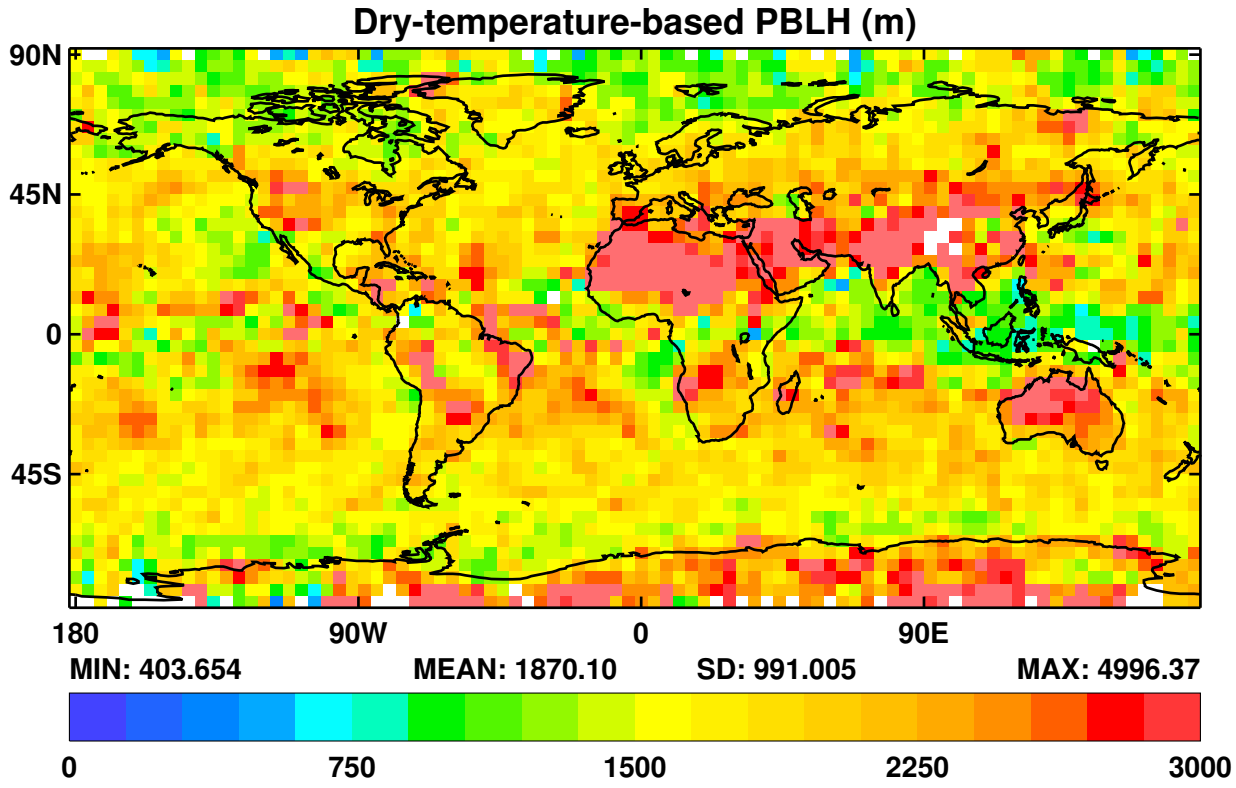

Figure 3.19: PBLH$_{T_{\mathrm{dry}}}$ derived from forward modelled Met Office backgrounds in April 2013, gridded at 4° resolution, smoothed 1–2–1 in both directions.

Global mean (forward modelled) PBLHs (km)

Nature	PBLH$_\alpha$	PBLH$_N$	PBLH$_{T_{\mathrm{dry}}}$	PBLH$_T$	PBLH$_q$	PBLH$_\rho$	PBLH$_{av}$
Strongest	N/A	1.5	1.9	1.7	1.4	1.9	1.7
Second strongest	N/A	2.3	2.5	2.5	2.2	2.4	2.4
Higher	N/A	2.5	2.9	2.9	2.5	3.0	2.8
Lower	N/A	1.2	1.4	1.4	1.1	1.3	1.2

Table 3.3: Global mean PBLHs calculated from forward modelled Met Office background fields, colocated with radio occultations in April 2013.

Distribution of the number of possible PBLHs (%)

No. of PBLHs	PBLH$_\alpha$	PBLH$_N$	PBLH$_{T_{\mathrm{dry}}}$	PBLH$_T$	PBLH$_q$	PBLH$_\rho$
Zero	100.0	75.6	74.6	1.2	0.0	1.2
One	0.0	3.6	1.2	6.2	3.8	3.7
Two	0.0	7.1	5.7	26.3	22.9	20.5
More than two	0.0	13.7	18.5	66.3	73.3	74.6

Table 3.4: Frequencies of possible PBLHs from forward modelled Met Office backgrounds in April 2013.

4 Summary, conclusions and future work

This report has discussed the planetary boundary layer height (PBLH) diagnostics that have been implemented in ROPP. Some early results have been presented, which make it clear that it would be incautious to rely on automatically generated PBLH products calculated according to the methods discussed in this report. Further development is essential before these PBLHs could be considered reliable measures of atmospheric boundary layer height.

The principal conclusions of this report are:

- The PBLH is characterised by large vertical gradients in observed bending angle, refractivity and dry temperature, and model temperature, specific humidity and relative humidity.
- Occasionally these locally enhanced gradients are strong enough to define a single reasonably reliable PBLH.
- Usually, however, there are several local maxima in the vertical gradients, each of which might just as easily define the PBLH. For this reason, the location of the second strongest local maximum is recorded by the PBLH diagnostics that have been recently introduced into ROPP. The number of possible PBLHs as diagnosed by local maxima in the vertical gradients — zero, one, two, or more than two — is also logged.
- Since a definitive quantitative *definition* of the PBLH is not available, the citing of a single number for the PBLH of a given RO profile seems to be of limited value. Instead, several PBLHs are calculated, from all the data that are available in the profile. The mutual consistency of this 'ensemble' of PBLHs helps the user to judge the likely reliability of the various measures.
- The number and nature of other possible PBLHs, arising from secondary extrema in vertical gradients in the profile, also influences the confidence in the given PBLH.
- Overall, the closest observationally based PBLH to the ERA-interim climatology is that based on refractivity. The lower of the two PBLHs derived from dry temperature could make a reasonable substitute.
- The closest model-based PBLH to the ERA-interim climatology is currently that based on specific humidity.
- PBLHs based on forward modelled background fields are, naturally, closer to PBLHs derived directly from background fields than to those derived from independent observations. They are also rather closer to the ERA-interim climatology, although this too is strongly dependent on model fields, of course. They share with the observations the property that PBLH_N is generally lower than $\mathrm{PBLH}_{T_{\mathrm{dry}}}$.

This preliminary report clearly raises more questions than it answers. It may therefore be prudent to focus further development work on better understood, and observed, boundary layer types. The marine stratocumulus regions are an obvious choice.

Some of that possible future work could include the following.

- An investigation of the sensitivity of the various PBLHs to vertical resolution, spatial location, the rising or setting of the occultation, the processing of the RO data in the lower troposphere, and so on.
- A study of the seasonal dependence of the diagnosed PBLHs. This should include a technical assessment of the seasonal variation of the relative reliability of the various PBLH diagnostics, as well as a scientific assessment of their utility in varous seasons, as determined by comparison with observations and/or climatology. This variability could guide the construction of uncertainties on the PBLHs — essential if, eventually, they are to be assimilated or used as reference dataset for model development.
- An investigation of the annual variation in the various PBLHs. This could also help in the estimation of PBLH uncertainties.
- The possible utility of these measures as climate data records would be worth assessing, as soon as the sensitivities discussed above are understood better. It would be straightforward to forward model the climate model into dry temperature, refractivity or bending angle space, from which a direct comparison with observationally derived PBLHs could be made.

Acknowledgements

Informative discussions with Gill Martin, Adrian Lock, Martin Willett and Mary Forsythe (UK Met Office) are gratefully acknowledged. Particular thanks are due to Chris Burrows (Met Office and ROM SAF) for the same, and for downloading the source RO data that were used in Section 3. Thanks also to Mary Forsythe, Roger Saunders and Kent Bækgaard Lauritsen for reviewing this report.

Bibliography

[1] Ao C O, Waliser D E, Chan S K, Li J-L, Tian B, Xie F and Manucci A J, Planetary boundary layer heights from GPS radio occultation refractivity and humidity profiles, Journal Geophys Res, **117**, D16117, 2012.

[2] ECMWF, IFS Documentation - Cy31r1. Part III: Dynamics and numerical procedures, http://www.ecmwf.int/sites/default/files/IFS_CY31R1_Part3.pdf, 2006.

[3] ECMWF, IFS Documentation - Cy40r1. Part IV: Physical Processes, http://www.ecmwf.int/sites/default/files/IFS_CY40R1_Part4.pdf, 2013.

[4] Garratt J R, Sensitivity of climate simulations to land-surface and atmospheric boundary-layer treatments — a review, Journal Clim, **6**, 419–448, 1993.

[5] Guo P, Kuo Y-H, Sokolovskiy S V and Lenschow D H, Estimating Atmospheric Boundary Layer Depth using COSMIC Radio Occultation Data, Terrestrial, Atmospheric and Oceanic Sciences, **11**, 1, pp53-114, 2000.

[6] Kursinski E R, Hajj G A, Leroy S S and Herman B, The GPS Radio Occultation Technique, Terrestrial, Atmospheric and Oceanic Sciences, **11**, 1, pp53-114, 2000.

[7] Lock A, private communication.

[8] Martin G, private communication.

[9] Ratnam M V and Basha S G, A robust method to determine global distribution of atmospheric boundary layer top from COSMIC GPS RO measurements, Atmos Sci Lett, **11**, 216–222, 2010.

[10] The Radio Occultation Meteorology Satellite Application Facility, http://www.romsaf.org, 2016.

[11] Simmons A, Uppala S, Dee D and Kobayashi S, ERA-Interim: New ECMWF reanalysis products from 1989 onwards, ECMWF Newsletter No. 110, 25–35, 2007.

[12] von Engeln A and Teixeira J, A ducting climatology derived from the European Centre for Medium-Range Weather Forecasts global analysis fields, Journal of Geophysical Research, **109**, D18104, doi:10.1029/2003JD004380, 2004.

[13] von Engeln A and Teixeira J, A Planetary Boundary Layer Height Climatology Derived from the ECMWF Reanalysis Data, Journal of Climate, **26**, 6575–6590, 2013.

[14] Xie F, Visiting Scientist Report 21: Investigation of methods for the determination of the PBL height from RO observations using ECMWF reanalysis data, SAF/ROM/DMI/REP/VS21/001, 2014.

ROM SAF (and earlier GRAS SAF) Reports

SAF/GRAS/METO/REP/GSR/001	Mono-dimensional thinning for GPS Radio Occulation
SAF/GRAS/METO/REP/GSR/002	Geodesy calculations in ROPP
SAF/GRAS/METO/REP/GSR/003	ROPP minimiser - minROPP
SAF/GRAS/METO/REP/GSR/004	Error function calculation in ROPP
SAF/GRAS/METO/REP/GSR/005	Refractivity calculations in ROPP
SAF/GRAS/METO/REP/GSR/006	Levenberg-Marquardt minimisation in ROPP
SAF/GRAS/METO/REP/GSR/007	Abel integral calculations in ROPP
SAF/GRAS/METO/REP/GSR/008	ROPP thinner algorithm
SAF/GRAS/METO/REP/GSR/009	Refractivity coefficients used in the assimilation of GPS radio occultation measurements
SAF/GRAS/METO/REP/GSR/010	Latitudinal Binning and Area-Weighted Averaging of Irregularly Distributed Radio Occultation Data
SAF/GRAS/METO/REP/GSR/011	ROPP 1dVar validation
SAF/GRAS/METO/REP/GSR/012	Assimilation of Global Positioning System Radio Occultation Data in the ECMWF ERA-Interim Re-analysis
SAF/GRAS/METO/REP/GSR/013	ROPP PP validation
SAF/ROM/METO/REP/RSR/014	A review of the geodesy calculations in ROPP
SAF/ROM/METO/REP/RSR/015	Improvements to the ROPP refractivity and bending angle operators
SAF/ROM/METO/REP/RSR/016	Simplifying EGM96 undulation calculations in ROPP
SAF/ROM/METO/REP/RSR/017	Simulation of L1 and L2 bending angles with a model ionosphere
SAF/ROM/METO/REP/RSR/018	Single Frequency Radio Occultation Retrievals: Impact on Numerical Weather Prediction
SAF/ROM/METO/REP/RSR/019	Implementation of the ROPP two-dimensional bending angle observation operator in an NWP system
SAF/ROM/METO/REP/RSR/020	Interpolation artefact in ECMWF monthly standard deviation plots
SAF/ROM/METO/REP/RSR/021	5th ROM SAF User Workshop on Applications of GPS radio occultation measurements
SAF/ROM/METO/REP/RSR/022	The use of the GPS radio occultation reflection flag for NWP applications
SAF/ROM/METO/REP/RSR/023	Assessment of a potential reflection flag product
SAF/ROM/METO/REP/RSR/024	The calculation of planetary boundary layer heights in ROPP

ROM SAF Reports are accessible via the ROM SAF website: http://www.romsaf.org